4
LOW-ENERGY PARTICLE POPULATION

S. M. Krimigis and E. C. Roelof

Voyager 1 and 2 performed the first unambiguous low-energy ($E \gtrsim 30$ keV) ion measurements in and around the Jovian magnetosphere in 1979. The magnetosphere contains a hot ($kT \sim 30$ keV), multicomponent (H, He, O, S) ion population dominated by convective flows in the corotation direction out to the dayside magnetopause and on the nightside to ~ 130–$150\ R_J$ beyond which the ion flow direction changes to predominantly antisolar, but with a strong component radially outward from Jupiter. This tailward flow of hot plasma, the magnetospheric wind, accounts for the loss of $\sim 2 \times 10^{27}$ ions/s and $\sim 2 \times 10^{13}$ W from the magnetosphere. Comparison of energetic ($\gtrsim 30$ keV) ion to magnetic field pressure reveals that particle and magnetic pressures are comparable from the magnetopause inward to at least $\sim 10\ R_J$, that is, magnetosphere dynamics is determined by pressure variations in a high-β plasma. This particle pressure is responsible for inflation of the magnetosphere and it (rather than the planetary magnetic field) determines the standoff distance with the solar wind. The ion spectrum can be described by a convected Maxwellian component at $E \lesssim 200$ keV, and a nonthermal tail at higher energies described by a power law of the form $E^{-\gamma}$. New theoretical techniques were developed in order to interpret the low-energy solid-state detector measurements of temperature, number densities, pressures, and flow velocities in this novel hot-plasma environment. Detailed analysis of composition measurements shows the presence of roughly equal numbers of protons and heavier ($A > 1$) ions, with likely charge states for the ions of He^+, O^{+2}, S^{+3}, and C^{+6}. In addition, molecular hydrogen (H_2 and H_3) has been identified, suggesting that the Jovian ionosphere is a source of magnetospheric plasma, in addition to the satellite sources of O and S. The ion spectra at $E \gtrsim 200$ keV/nucleon are best organized in terms of energy/charge, suggesting an electric field acceleration mechanism. Finally, measurement of convection velocities shows that the plasma is more or less corotating at large ($\gtrsim 30 R_J$) distances from Jupiter, but slows to well below corotation closer to the planet.

4.1. Introduction

Our knowledge of Jupiter's magnetosphere before the Pioneers and Voyagers actually flew by the planet was conveyed to us by relativistic electrons. Those trapped in the Jovian radiation belts produce the decimetric and decametric radio emissions (see Chap. 5) first detected at Earth in the 1950s, and those electrons escaping into interplanetary space fill the heliosphere and dominate the galactic component up to energies of ~ 40 MeV. However, our experience with the Earth's magnetosphere has shown that its dynamics are primarily determined by energetic ions in the range of tens to hundreds of keV. For example, the energy density in the ring current consists primarily of ions in the range of 20–200 keV [Williams, 1979], whereas the dynamics of the magnetotail are primarily determined by plasma flows in the range of a few keV to several tens of keV [Frank, Ackerson, and Lepping, 1976; Keath et al., 1976; Roelof et al., 1976; Coroniti et al., 1980b]. At Jupiter, the low-energy ions dominate magnetospheric processes even more dramatically than at Earth. Consequently, although we shall not ignore the low-energy electrons altogether, our main interest concerns the discovery by Voyager of the crucial roles played by ions $\lesssim 1$ MeV/nucleon in Jupiter's huge and complex magnetosphere.

Magnetic field and energetic particle measurements obtained during the Pioneer 10 and 11 encounters with Jupiter in 1973 and 1974, respectively, revealed substantial information concerning the morphology and overall structure of the Jovian magnetosphere. Some of the most important findings included the sustained 10-hr periodicity in particle fluxes and magnetic field magnitude, and the overall inflation of the magnetosphere to distances that were twice as large as those predicted using the magnitude of the Jovian dipole moment measured by the spacecraft. An excellent review and synthesis of the Pioneer results published through 1977 is contained in a paper by Kennel and Coroniti [1979]. The Pioneer instrumentation, however, did not include detectors capable of obtaining comprehensive ion measurements in the energy range of a few keV to several hundred keV, so that the characteristics of the low-energy ($\lesssim 200$ keV) ion component of the magnetospheric particle population (which was presumably responsible for the inflation of the magnetosphere), and its composition remained largely unknown. As a consequence, questions of the dynamics and the overall balance between the magnetic field and plasma population in the magnetosphere of Jupiter could only be speculated upon [Walker, Kivelson, and Schardt, 1978; Goertz et al., 1979].

In what follows, we review and interpret measurements of the intensities, energy spectra, angular variations, and composition characteristics of the low-energy ion population obtained by both Voyager spacecraft in the Jovian magnetosphere. We also describe some novel analysis techniques that we have employed to generate density, pressure, composition, and plasma-flow profiles in the magnetosphere, and we compare these to results reported by other investigations on the spacecraft.

The energetic ion component of the Jovian magnetosphere provides most of the plasma pressure and thus determines the dynamics of magnetospheric motions. In this sense, the magnetosphere of Jupiter is unique among those with intrinsic magnetic fields (i.e., Mercury, Earth, and Saturn), in that these particles rather than the magnetic field provide the primary pressure for deflecting the solar wind. In addition, these ions account for a substantial fraction of the plasma number density in the outermost portion of the magnetosphere and represent a significant part of the number density at distances as close as $\sim 10\ R_J$ to the planet. The composition of the energetic ion population is dominated by hydrogen, helium, oxygen, and sulfur, the heavier ions being present in amounts comparable with the protons. Measurements of the ion flux anisotropies show that these are dominated by convective flows in the corotation direction on the dayside inside the magnetopause, and on the nightside to distances of ~ 130–$150\ R_J$; beyond this point, to distances well past the dawn bow shock of the planet, the ion flows change predominantly to the antisolar direction, but with a strong component projected radially outward from the planet.

4.2. Observational overview

The Low-Energy Charged Particle (LECP) investigation on the Voyager spacecraft utilizes a variety of solid state detectors in the LEMPA (Low-Energy Magnetospheric Particle Analyzer) head to obtain measurements of energetic electrons (14 keV $\leq E_e \lesssim 20$ MeV) and ions (30 keV $\leq E_i \leq 150$ MeV) in several energy intervals with good energy, species, time, and spatial resolution. Above an energy of ~ 200 keV/nucleon, individual ion species can be identified separately and their energy spectra and angular distributions determined using the LEPT (Low-Energy Particle Telescope) head. Sensor geometry factors range from $\sim 2 \times 10^{-3}$ cm^2 sr to ~ 2.3 cm^2 sr and are designed to handle fluxes ranging from quiet-time cosmic ray medium nuclei ($< 10^{-6}$ cm^2 s sr)$^{-1}$ to intense proton and electron populations ($> 10^8$ cm^2 s sr)$^{-1}$ in the inner

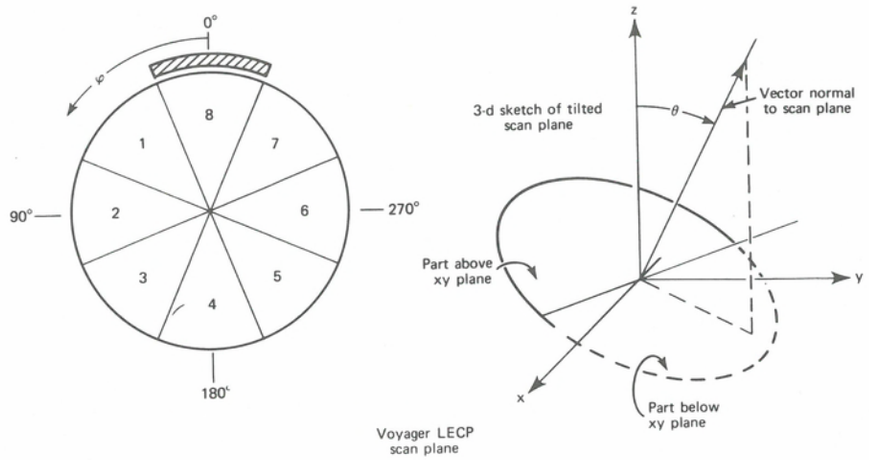

Fig. 4.1. Voyager LECP scan plane: (*a*) scan plane sectoring and angle conventions (angles are measured counterclockwise from the center of the shield sector (sector 8)); and (*b*) three-dimensional sketch indicating how scan plane is tilted from the Jupiter ecliptic xy plane. When Voyager is oriented on the star Canopus, the polar angle $\theta \sim 100°$. The z axis points toward the north ecliptic pole [Carbary et al., 1981].

Jovian magnetosphere. A full description of the instrument design characteristics and capabilities have been given elsewhere [Krimigis et al., 1977, 1981].

The LECP detector heads are mounted on a rotating platform on the spacecraft so that angular measurements in eight 45° intervals may be obtained. Figure 4.1 shows the rotation plane of the detector telescopes where the x and y axes lie roughly in the ecliptic plane. The sector scheme in the rotation plane of the instrument is shown on the left side and depicts the eight 45° sectors. The detector apertures can be rotated through 360° in 45° steps at rates ranging from 1 step every 6 s to 1 step every 48 s; it is also possible to park the detector in any one of the eight sectors. Sector 8 is permanently blocked by a shield so that an accurate estimate of background contributions to the count rate of every channel can be obtained once per scan. The viewing directions of each sector depend on the particular spacecraft orientation. These directions are shown in Figure 4.2 for two of the most common spacecraft references, that is, the stars Canopus and Arcturus. The lower part of the figure shows the viewing directions for most of the Voyager 2 encounter, indicating that the LECP instrument was viewing directions quite close to the ecliptic plane. The tick marks at the zero latitude line labeled by day number indicate the direction of corotation on that particular day. It is evident from the upper part of Figure 4.2 that the Arcturus reference is not optimum for measuring corotational flow in the Jovian magnetosphere. This orientation occurred on days 192–195 during the Voyager 2 encounter and for most of the outbound pass of the Voyager 1 encounter.

The LECP instruments on Voyager 1 and Voyager 2 detected the approach to Jupiter's magnetosphere through a number of upstream ion intensity enhancements several hundred R_J before encounter of the planetary bow shock. A trajectory plot indicating the time and location of each ion event observed inbound from both spacecraft and outbound from Voyager 1 is shown in Figure 4.3 [Zwickl et al., 1980; 1981]. The solid circles represent the location of measurements of short-lived events lasting from a few minutes to three hours in the low-energy ($\gtrsim 50$ keV) ion channels. The solid

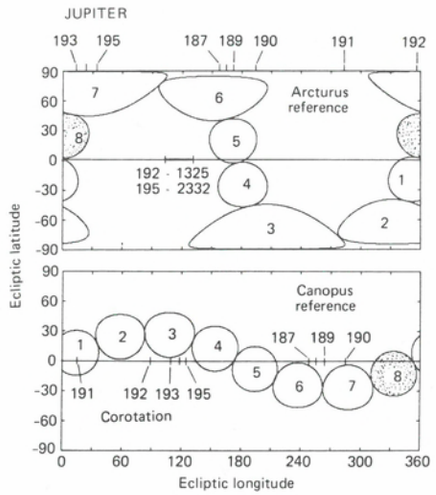

Fig. 4.2. Viewing of the LECP sectors in ecliptic coordinates. Shown are the viewing areas for the eight LECP sectors when the Voyager 2 spacecraft was in the Arcturus reference orientation (top panel) and in the Canopus reference orientation (lower panel). The corotation direction at 0000 UT of each day is given by the tick marks on the zero latitude line. The Jupiter direction for each day is given at the top of the figure. The viewing directions for the Voyager 1 instrument are effectively the same as shown here [Krimigis et al., 1981].

squares in Figure 4.3 represent long-lived flux increases that last at least 8 hr. Figure 4.3 also shows two mass histograms of ions in the range ~0.6 to 1 MeV/nucleon; the one on the left was obtained in the magnetosheath whereas the one on the right was measured during one of the upstream events. The upstream event contained substantial enhancements of oxygen and sulfur, similar to the composition in the magnetosheath and magnetosphere [Hamilton et al., 1981].

The measurements obtained by the LECP instrument in the magnetosphere and its vicinity have been synthesized into a phenomenological model [Krimigis et al., 1979b, 1981], which is shown in Figure 4.4. Here an attempt is made to present the three-dimensional view of the magnetosphere surface. The horizontal transparent plane represents the ecliptic plane, and the rotating magnetodisc at this particular orientation of the planetary magnetic-moment vector appears on the nightside below this plane. The arrows indicate the direction of the corotational plasma flow in the magnetodisc, and its wavy nature suggests a propagating Alfvén wave. The large arrows to the right indicate the direction of solar-wind flow. The bulge in the magnetodisc at about 0800 local time has been exaggerated to indicate the possibly irregular nature of the plasma boundary/magnetopause surface owing to variation in solar wind pressure. Beyond the nightside corotational boundary, the small arrows indicate plasma outflow in the magnetospheric wind, which flares out and expands beyond the nominal width of the nightside magnetodisc.

In the following overview, we present data that are to be viewed in the context of the concepts incorporated in the schematic view of the magnetosphere in Figure 4.4. Figure 4.5 presents the averages of selected energy channels from the Voyager 1 LECP instrument for a 40-day period, beginning at distances $>200\ R_J$ inbound and extending to $>350\ R_J$ outbound. In the top curve, the intensity of the low-energy ions ($Z \geq 1$), begins to increase inside $\sim 200\ R_J$, long before the spacecraft encountered the planetary magnetopause. These discrete increases are emissions of magnetospheric ions and are discussed in detail by Zwickl et al. [1981]. The overall increase in rate is well over six orders of magnitude for the data shown, not including the particle intensities at closest approach, which will be presented separately.

Following periapsis, the basic asymmetry of the magnetosphere between day and night begins to manifest itself with the first encounter of the nightside magnetodisc occurring at $\sim 22\ R_J$; these encounters continue in a periodic fashion with a 10-hr

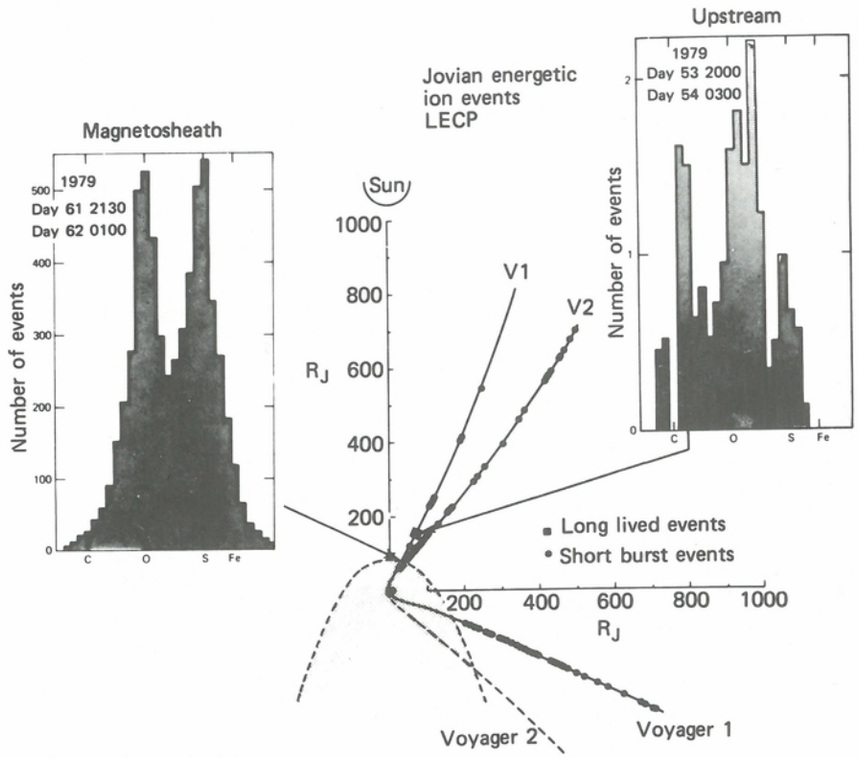

Fig. 4.3. Voyager 1 and 2 trajectories within 1000 R_J of Jupiter. Shaded region around Jupiter represents the area encompassed by the bow shock as measured by Voyager 1. The increased number of events measured by Voyager 2 inbound and by Voyager 2 outbound strongly suggests that interplanetary field-line connection to the bow shock is necessary for the observation of Jovian energetic ion events in interplanetary space. Voyager 2 outbound data are not included because of poor data quality during solar conjunction. The orientation of the eight LECP look directions are shown inbound and outbound with respect to the Sun, the nominal direction of the magnetic field and Jupiter [Zwickl et al., 1981].

period to $\sim 130\ R_J$. Various discontinuities in the basic structure are apparent at ~ 55–$60\ R_J$, at ~ 80–$90\ R_J$, and finally at $\sim 130\ R_J$ where the basic periodicity breaks down prior to the encounter of the magnetopause at $\sim 160\ R_J$. We note that activity in the intensity profile of low-energy ions continues to at least $350\ R_J$, long after magnetopause passage.

The second data trace in the top panel shows the intensity profile of uniquely identified protons ($Z = 1$). The proton profile is grossly similar to that of the ions ($Z \geq 1$) although there exist significant differences; in particular, the decrease in proton intensity to interplanetary values soon after the spacecraft entered the magnetosheath from the nightside of the planet is in contrast to the continued presence of low-energy ions. The third curve represents ions with $Z \geq 6$ which are judged to be a combination of sulfur and oxygen by extrapolation from high-energy channels [Krimigis et al., 1979a]. Again, the gross structure of the intensity profile is similar to that of lower energy ions and of the protons but with some notable exceptions. For example, the overall increase in the ion profile is well over seven orders of magnitude, that is, larger than that of

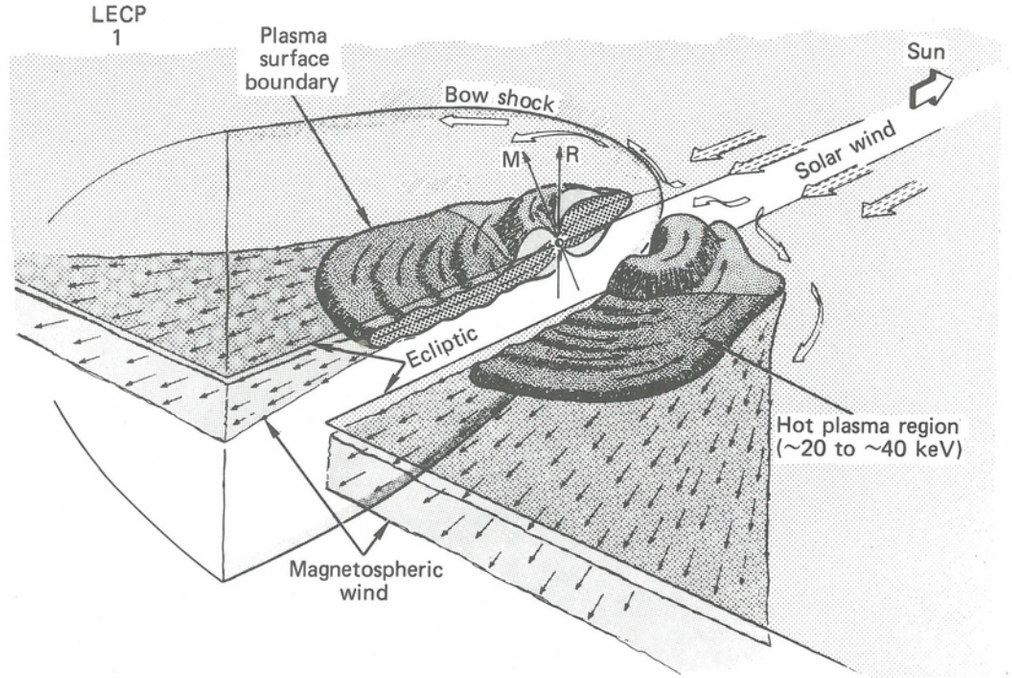

Fig. 4.4. The hot plasma model of the Jovian magnetosphere gives a three-dimensional view. The grey region denotes the hot plasma of the corotating magnetodisc. Solar-wind pressure (arrows), causes the disc to be blunt on the dayside and extended on the nightside. In the far magnetotail (thin arrows), the disc is disrupted and particles are expelled away from the planet in the magnetospheric wind. The temperature of the plasma in most of the outer magnetosphere is 20–40 keV.

protons; in addition, it is possible to deduce that the overall ion intensity increases began as early as day 51, long before the spacecraft encountered the Jovian bow shock for the first time. The relative increase in these ions towards the end of day 60 was greater than that of protons or lower-energy ions. Following the breakdown in periodicity at $\sim 130\ R_J$, the $Z \geq 6$ ions resemble more the profile of the low-energy ions ($Z \geq 1$) than of the protons.

The middle panel of Figure 4.5 shows the profile of low-energy electrons, which generally exhibit the same gross behavior as the ions, although the upstream increase on days 53 and 54 is not clearly evident in the electrons; also, the downstream intensity increases observed for the ions are not always present in the electrons. The electrons, however, continue to be detected far beyond the nominal magnetopause crossing, but terminate abruptly at the first bow-shock crossing on day 77 and later at the shock crossing on day 81.

Finally, the bottom panel on the figure presents the proton to alpha particle (p/α) ratio in the indicated energy range for the duration of the encounter, with the exception of the period around closest approach. The ratio has relatively large values (~ 50–80) even before encounter of the Jovian magnetopause with the largest values (~ 200) obtained at the end of day 53. Generally, the ratios within the magnetosphere, and especially outbound out to the end of day 70 are larger than typically observed in the solar wind or solar-energetic-particle events (~ 10–30).

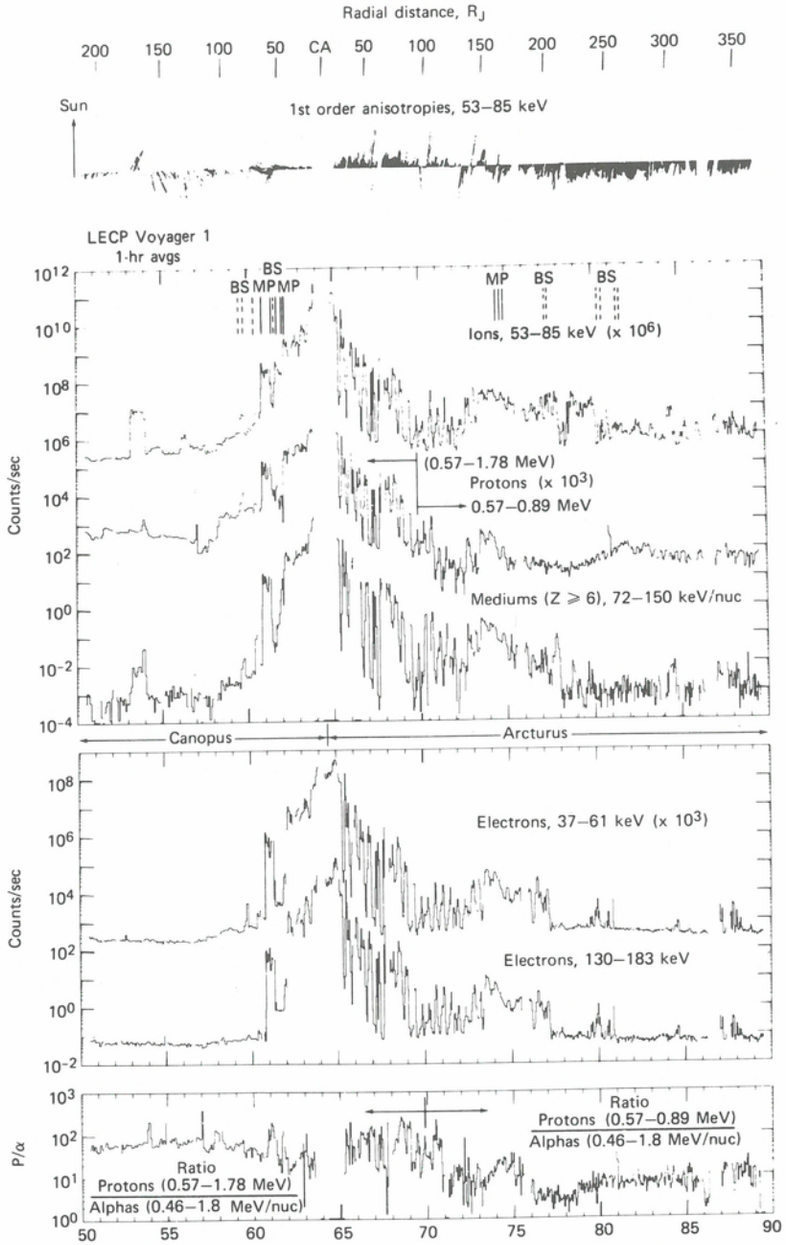

Fig. 4.5. Overview of Voyager 1 encounter. Plotted in the two center panels are 1-hr averages of several of the LECP ion and electron channels. In addition, the anisotropy of the low-energy ions is plotted at the top of the figure while the p/α ratio is at the bottom. Energetic particles from the Jovian magnetosphere were first detected at a distance of $>600\ R_J$ inbound and extended to $>1500\ R_J$ outbound [Zwickl et al., 1981]. The spacecraft entered the magnetosphere initially on day 60 and remained inside until ~ day 75. Closest approach to the planet occurred at ~1200 UT on day 64. The asymmetric nature of the sunward and tailward magnetosphere [Fillius, 1976] is clearly evident as is the corotational nature of the anisotropy.

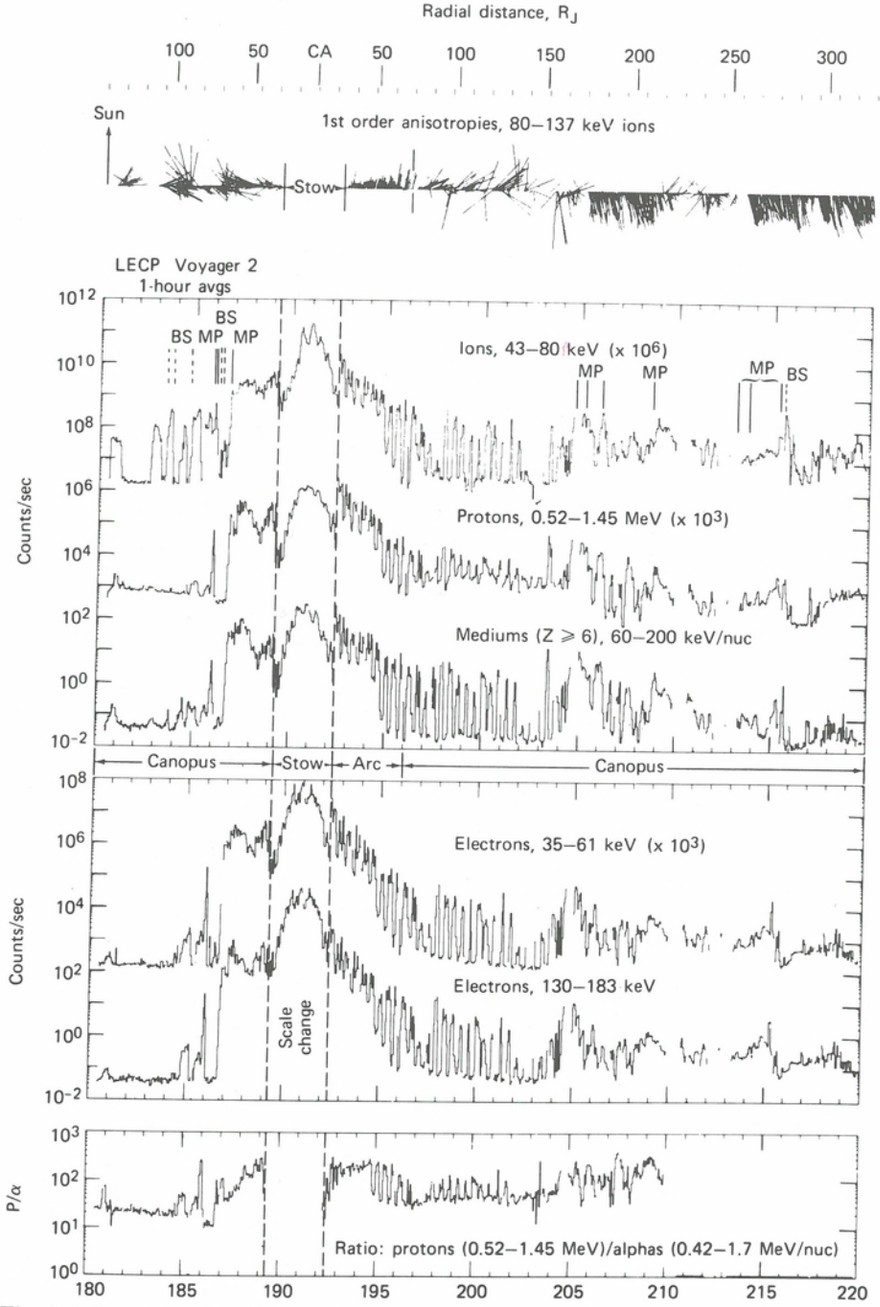

Fig. 4.6. Overview of the Voyager 2 encounter. The format here is the same as in the previous figure. Voyager 2 periapsis occurred at ~2300 UT on day 190. During the interval 189, 0540 UT through 192, 1345 UT, the LECP instrument was in a non-stepping "stow" mode to reduce the counting rate so that compositional measurements could be made through closest approach. As in Figure 4.5, the corotation nature of the anisotropy during intervals when the spacecraft was in the magnetosphere is clearly evident.

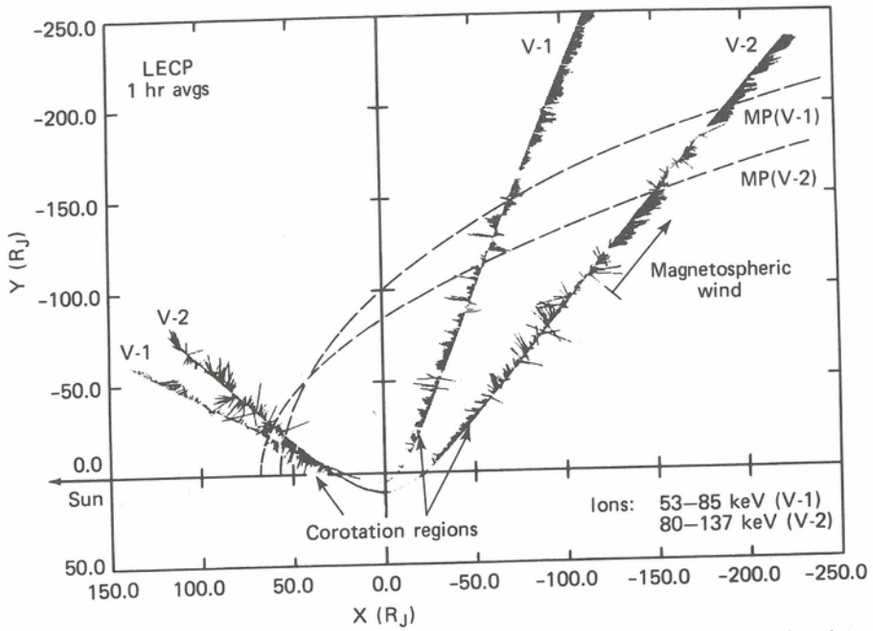

Fig. 4.7. Summary of the anisotropy [Krimigis et al., 1981]. Flows in the corotational directions were observed by both Voyager 1 and 2 throughout the inbound leg of magnetosphere passage and out to 130–160 R_J on the outbound legs. Beyond this distance, the flow changed to an antisunward/anti-Jupiter direction. The dashed line gives the model magnetopause locations for both encounters [Ness et al., 1979c].

The delineation of different regions of the Jovian magnetosphere environment is evident from the ion anisotropy data shown at the top of Figure 4.5 in the form of vectors. These vectors, obtained to first order by a harmonic fit to the sector data [Carbary et al., 1981], point in the direction of particle flow. Note the abrupt flow change to a direction away from the Sun coincident with the breakdown in periodicity at $\sim 130\ R_J$, but prior to the first magnetopause crossing. We take this to be the spacecraft entry into the magnetospheric wind indicated in Figure 4.4.

Figure 4.6 presents data from the Voyager 2 encounter using the same format as that for Voyager 1. The top curve in the upper panel shows significantly more upstream ion activity during this encounter. This difference is probably due to the fact that the interplanetary field connection from the spacecraft to the Jovian bow shock is more likely to occur for the trajectory of Voyager 2, because the field tends to be nearly transverse to the Jupiter–Sun line (see Fig. 4.3). The gross intensity profile has many features similar to those seen by Voyager 1 including the breakdown in periodicity at $\sim 150\ R_J$ and continued low-energy ion intensity fluctuations downstream to at least 340 R_J. Note the large enhancement of $Z \geq 6$ ions relative to that of protons on day 203. This marks the first change in the plasma flow from the corotational to the tailward direction (vector trace on top). As was the case for Voyager 1, the p/α ratio is larger than typical solar wind or solar-interplanetary particle values. In both Figures 4.5 and 4.6, the transition to the magnetospheric wind shown schematically in Figure 4.4 is evident and coincident with the breakdown in periodicity inside the magnetopause. Note that the p/α ratio in the magnetospheric wind region closely resembles that of the inner part of the magnetosphere and is at least an order of magnitude higher than values expected in the solar wind.

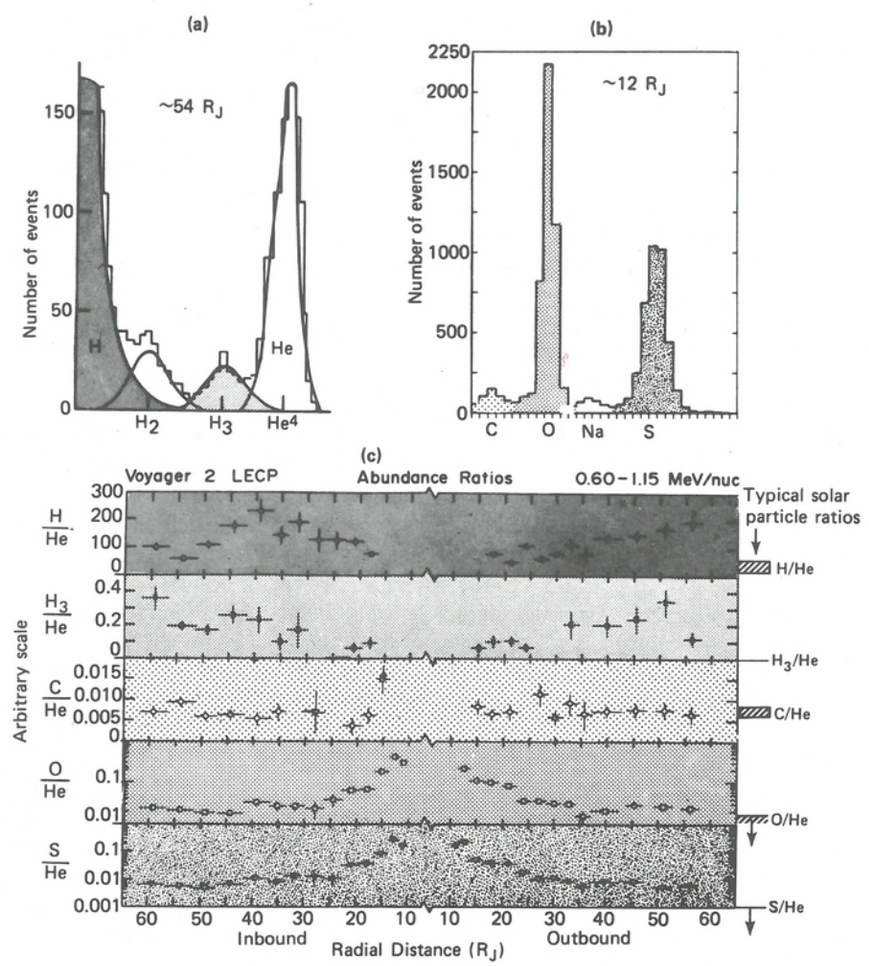

Fig. 4.8. Elemental composition measurements by the LECP instrument within the Jovian magnetosphere: (*a*) mass histogram showing the presence of molecular hydrogen, H_2 and H_3; (*b*) mass histogram representative of the composition throughout the magnetosphere; and (*c*) variation with distance to the planet of the abundances of the elements indicated relative to He (adapted from Krimigis et al. [1979a,b] and Hamilton et al. [1981]). Solar abundances are shown on the left-hand ordinate for comparison.

A most revealing view of the structure of the magnetosphere is provided by the first-order ion anisotropies, which can be taken as indicative of convective plasma flow direction. A summary of the overall anisotropy profile at low energies for both Voyagers 1 and 2 is presented in Figure 4.7 in a more convenient format. Here the projections of the first-order-anisotropy vectors onto the ecliptic plane are drawn on the spacecraft trajectories from $\sim 150\ R_J$ upstream to $\sim 325\ R_J$ downstream of the planet. The model magnetopause locations from both encounters [Ness et al., 1979c] are shown for reference. We note that there exist two general flow directions in the Jovian magnetosphere, one which points in the direction of planetary corotation and obtains throughout the dayside, and on the nightside to distances of ~ 130–$160\ R_J$; beyond that distance and before crossing the magnetopause (identified by the plasma instru-

ment [Bridge et al., 1979a,b]), the flow changes to an antisunward/anti-Jupiter direction and continues to large distances away from the planet. These results are the basis for the schematic representation of corotational flow and antisunward flow in Figure 4.4.

The composition characteristic of most of the Jovian magnetosphere at higher energies is presented in Figure 4.8. Figure 4.8*a* shows a histogram of the light elements which reveals the presence of molecular hydrogen (H_2,H_3) in addition to the expected peaks of hydrogen and helium [Hamilton et al., 1980]. The presence of H_3 which is expected to be a constituent of the Jovian upper ionosphere is taken as evidence that the ionosphere is a significant plasma source, [as originally suggested by Ioannidis and Brice, 1971], at least for the outer part of the Jovian magnetosphere. The ionospheric source of hydrogen may well be the cause of the large values of the H/He ratios shown in Figure 4.6. Figure 4.8*b* shows a histogram of heavier ions [Krimigis et al., 1979b; Hamilton et al., 1981], which reveals the presence of peaks at the location of carbon, oxygen, sodium, and sulfur, and is characteristic of the composition throughout the Jovian magnetosphere. As pointed out previously O, S, and Na originate at Io (see also Chap. 3).

Figure 4.8*c* presents the ratios of five different species relative to helium, computed over equal energy/nucleon intervals near ~ 1 MeV/nucleon. We note three basic types of behavior. He and H_3 both decrease relative to helium with decreasing radial distance, except for a period between 60 and 40 R_J inbound. The C/He ratio remains essentially constant throughout the magnetosphere. Both O and S increase rather smoothly relative to He with decreasing distance within ~ 30–40 R_J. The magnitude of the ratio change from outer to inner magnetosphere is much larger for O and S than for H and H_3 (note the logarithmic scale for the oxygen and sulphur ratios).

As pointed out by Krimigis et al. [1979b], the C/He ratio observed by Voyager 2 in Jupiter's magnetosphere is quite similar to that found in solar particles. The O/He ratio in the outer magnetosphere is about a factor of 2–3 higher than for solar particles. On the other hand, S/He is more than a factor of 10 higher than solar values even in the outer magnetosphere. These facts, plus the fact that the O/He and S/He ratios increase as Voyager 2 approached Jupiter although the C/He ratio remains constant, led Krimigis et al. [1979b] to suggest that the energetic C and He are of solar origin (probably from the solar wind), that S is of local origin (probably from Io), whereas O could have both a local and solar component. Because H_3 has not been observed among solar particles, its local origin is certain.

The H/He ratio was quite large in the outer Jovian magnetosphere, typically >100. This is certainly a much larger value than found in the solar wind (typically 10–20) although, as will be discussed later, the nature of the acceleration process can greatly alter the abundance ratio in the source material. Because H_3 is of ionospheric origin, Hamilton et al. [1980] have argued that H^+ ions should also participate in the processes that bring H_3^+ ions from the ionosphere. Helium, on the other hand, may not participate in these processes because it is found lower in the Jovian atmosphere. This would explain the large hydrogen to helium ratios.

To illustrate the ion spectral form at low energies, we show in Figure 4.9 a typical spectrum measured in the outer magnetosphere by Voyager 2. The shape of the spectrum does not conform with a power law over the entire energy range, but rather exhibits significant flattening at the low-energy end. Although ions are not specifically identified at lower energies (round points), the detector response at 90° to the flow direction is generally due to protons [Krimigis et al., 1981]; the pulse height analyzed proton spectrum (dashed line) and a square point that represents a specific proton rate

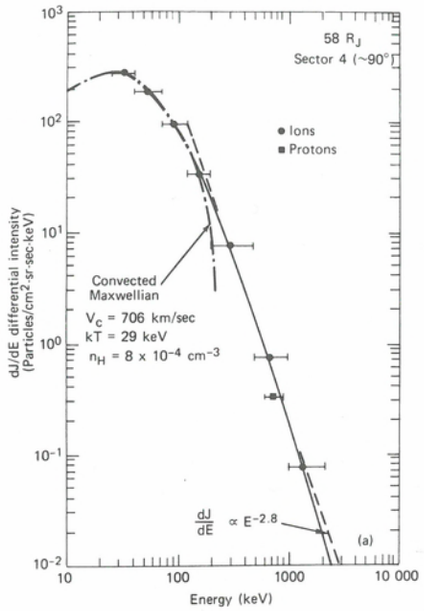

Fig. 4.9. Detailed spectral fit to the low energy ion channels [Krimigis et al., 1981]. Plotted (closed circles) are the intensities measured in sector 4 ($\sim 90°$ from convection direction) of the low energy ion channels. In this direction, the detector response is thought to be due to protons only. The dotted curve shows the thermal distribution obtained using parameters listed in the figure. The dashed curve indicates a power-law fit from the pulse-height-analyzed proton data with a spectral index of 2.8. The closed square is from the composition detector head channel, which is sensitive only to protons.

from the composition detector support this conclusion. Assuming that the detector is responding to protons at all energies, we proceed to obtain a fit to the three lowest energy points by assuming a convected Maxwellian distribution [Krimigis et al., 1979a]. The parameters providing the best fit are a velocity of ~ 700 km s^{-1}, temperature of ~ 29 keV and density of $\sim 8 \times 10^{-4}$ cm^{-3}. Similar temperatures have been obtained for most of the magnetosphere for both encounters and represent the basis for labeling the magnetodisc in Figure 4.4 with the temperature of 20–40 keV.

The importance of the information contained in the spectrum and composition of the low-energy charged particle populations inside and outside the Jovian magnetosphere should now be apparent. The process of deducing this information from the LECP measurements requires some understanding of how such an instrument responds to hot, flowing, multispecies plasma. The necessary techniques are described in the next section.

4.3. Measurement of hot multispecies convected plasmas using energetic particle detectors

The surprise for the LECP team when the data came back from the Voyager 1 Jupiter encounter was not that LECP had responded to thermal plasma in the outer magnetosphere, but rather that there was such a relatively dense ($\sim 10^{-3}$ cm^{-3}) plasma component with so high a temperature ($kT \simeq 20$ keV) that was so rich in heavy ions (like oxygen and sulfur). To see why we expected the LECP to respond to plasmas, even if the temperature had been considerably lower and the magnetosphere even less rich in heavy ions, we have to examine in some detail the response of a total energy detector to a moving plasma.

Well before the Voyager 1 encounter with Jupiter's magnetosphere, we were aware that solid state detectors with low electronic thresholds ($\lesssim 30$ keV) could respond to flowing hot plasmas of sufficiently high density [Roelof et al., 1976]. In the Earth's plasma sheet and magnetosheath, there are strong, sporadic proton plasma flows with

bulk velocities (V) of several hundred km s^{-1}, densities in the range 10^{-3}–10^{-1} cm^{-3} and temperatures (T) of several keV (where the thermal energy kT may be expressed in eV using the relation $10^6\ K = 86$ eV). Direct plasma measurements had been made with electrostatic analyzers on the IMP-6, 7, and 8 spacecraft, for example, Frank, Ackerson, and Lepping [1976] and Hones [1976]. Also on the IMP-7 and 8 spacecraft were energetic particle detectors [Williams, 1977] that had an energy threshold for incident protons of ~50 keV: 30 keV electronic threshold for energy deposited in the live volume of the detector, with an additional ~20 keV undetected energy loss in the dead layer and the ~40 micrograms cm^{-2} aluminum contact. Unlike the electrostatic analyzers, which respond at considerably lower energies to the bulk of the thermal plasma, the solid state detectors usually respond to the high-energy tail of the plasma distribution. In the Earth's plasma sheet, we showed that this tail contained sufficient information to provide estimates of plasma temperature and bulk velocity from the angular and spectral response of the IMP detectors [Roelof et al., 1976]. Once we understood the conditions that exist in Jupiter's magnetosphere, we realized that the Voyager LEMPA detectors could yield estimates not only of temperature and bulk velocity, but also of lower bounds on density and pressure.

It is the motion of the plasma that dramatically enhances the response of an energetic particle detector. The energy of a thermal particle with relative velocity v, averaged over the distribution function for a plasma with temperature T flowing with a bulk velocity $\mathbf{V}$, is

$$<E> = \frac{m}{2} < (\mathbf{V} + \mathbf{v})^2 > = mV^2/2 + 3\,kT/2 \tag{4.1}$$

because $\langle v^2 \rangle = 3\,kT/m$. A handy relationship to remember is that an ion with instantaneous velocity v (expressed in km s^{-1}) has an energy per nucleon given by $(v/439\ \text{km s}^{-1})^2$ in keV/nucleon. Equation (4.1) then immediately illustrates how bulk motion of a thermal plasma greatly enhances the detector's sensitivities to the heavier species. For a plasma with $kT = 20$ keV and a bulk velocity $V = 600$ km s^{-1}, protons have a translation energy $mV^2/2 = 1.9$ keV, which is considerably smaller than their mean thermal energy $3\,kT/2 = 30$ keV. By contrast, even though oxygen ions (^{16}O) at the same temperature also have 30 keV mean thermal energy, their energy of translation adds another 30 keV to their total mean energy.

Thinking in terms of Jupiter's magnetodisc, if the hot plasma component "corotates" with the planet's ionosphere, then the magnetic field lines are "rooted" in the conducting ionosphere in the sense that the polarization electric field $\mathbf{E} = -(\mathbf{V} \times \mathbf{B})/c$ maps out from the ionosphere into the magnetodisc along the magnetic field lines. Thus, at radius $\mathbf{r}$ where $\mathbf{V} = \Omega \times \mathbf{r}$ (Ω being the Jovian System III angular velocity of 1.76×10^{-4} s^{-1}), the $\mathbf{E} \times \mathbf{B}$ drift velocity of a charged particle would be $\mathbf{V} = (c/B^2)(E \times B) = \Omega \times \mathbf{r} - \hat{\mathbf{B}}\,\hat{\mathbf{B}} \cdot (\Omega \times \mathbf{r})$, the second term vanishing if the field lines lie in meridional planes. In the equatorial plane, $V = |\Omega \times \mathbf{r}| = \Omega r = (12.6\ \text{km s}^{-1})(r/R_J)$, so the radius at which the translation energy term in Equation (4.1) equals the mean thermal energy would be $(42.7\ R_J)\,(kT/A)^{1/2}$, where kT is expressed in keV and A is the atomic mass number of the ions. Thus, for $kT = 20$ keV, the corotation energy of hydrogen is negligible compared to its thermal energy within the magnetosphere, but the corotation and thermal energies are comparable for ^{16}O at 47.7 R_J, or for ^{32}S at 33.8 R_J.

An aside may be appropriate here: we have assumed that all ion species have the same temperature and the same bulk velocity, and indeed our LECP results for Jupiter appear to be approximately self-consistent within this assumption. However, in another space plasma (the solar wind near 1 AU), it is a better approximation to say that all ion species have about the same mean-square velocity. Because $\langle v_a^2 \rangle = 3\,kT_a/m_a$ for species "a" with atomic mass number A, equal thermal speeds would imply $T_a \simeq A\,T_H$, where T_H is the hydrogen temperature. Moreover, the bulk velocities $\mathbf{V}_a$ can differ from the hydrogen bulk velocity $\mathbf{V}_H$ by a velocity increment $\Delta\mathbf{V}_a$ which is magnetic-field aligned and seems to be bounded above by the local Alfvén velocity. These results were established for solar wind ^4He by Asbridge et al. [1976] and Marsch et al. [1982] and recently extended to solar wind ^{56}Fe by Mitchell and Roelof [1980] and Mitchell et al. [1981].

The discussion above of mean thermal and translational energies was intended only as an introduction and is hardly a complete discussion of what an energetic particle detector actually measures. What we must examine is the instrumental response to the incident unidirectional differential flux $j_a(E, \mathbf{p})$: the number of particles of species "a" with energies in the differential range $(E, E + dE)$ and momenta $\mathbf{p}$ in a differential solid angle $d^2\omega$ about the unit vector $\mathbf{p}$ crossing an area $d^2\sigma$ (normal to $\mathbf{p}$) per unit time is $j_a\,dE\,d^2\omega\,d^2\sigma$. From the measurements, we can estimate the temperature, number density, pressure, and convection velocity of the dominant hot ions.

To put things on a solid theoretical ground, we begin with the phase space density function $f^a(\mathbf{x}, \mathbf{p})\,d^3x\,d^3p$ which gives the number of particles of species "a" in a volume d^3x about position $\mathbf{x}$ and with momenta in the range $d^3p = p^2\,dp\,d^2\omega$ centered about $\mathbf{p}$. The unidirectional flux function $j^a(E, \mathbf{p})$, which we have been using is just the velocity v times the number of particles in the volume d^3x about $\mathbf{x}$ in the energy range $dE = v\,dp$ with momenta in d^3p about $\mathbf{p}$:

$$j^a(E,\hat{\mathbf{p}})\,d^3x\,dE\,d^2\omega = vf^a(\mathbf{x},\mathbf{p})\,d^3x\,p^2\,dp\,d^2\omega \tag{4.2}$$

from which we obtain the useful relationship

$$j^a(E,\hat{\mathbf{p}}) = p^2 f^a(\mathbf{x},\mathbf{p}) \tag{4.3}$$

Allow us a slight lapse from rigorous notation in not being explicit about the $\mathbf{x}$ dependence of j^a because we usually are talking about the measured flux at the spacecraft, and we always know where that is.

One consequence of the covariance of the laws of statistical mechanics is that the phase space density is invariant under the Lorentz transformation. Using the nonrelativistic (Galilean) limit for the velocity transformation $\mathbf{v} = \tilde{\mathbf{v}} + \mathbf{V}$, where $\mathbf{v}$ is the velocity of a particle in the rest frame (e.g., the spacecraft), and $\tilde{\mathbf{v}}$ is the velocity which the same particle would have in a frame moving with velocity $\mathbf{V}$ relative to the rest frame, the equality of the distribution function in the spacecraft frame $f^a(\mathbf{x},\mathbf{p})$ to the distribution function $\tilde{f}^a(\tilde{\mathbf{x}},\tilde{\mathbf{p}})$ in a frame moving with the bulk velocity of ion plasma species "a" implies, from (4.3), that at the same point in configuration space, the fluxes are related by

$$j^a(E,\hat{\mathbf{p}})/p^2 = \tilde{j}^a(\tilde{E},\tilde{\mathbf{p}})/\tilde{p}^2 \tag{4.4}$$

where $\tilde{E} = \tilde{p}^2/2m_a$ and $\tilde{p}^2 = m_a^2\,(v^2 - 2\mathbf{v} \cdot \mathbf{V} + V^2)$ for a given ion species.

The transformation, (4.4), of fluxes (valid also when the relativistic momentum transformation is used), finds many applications in energetic particle space physics. In our discussion, its main utility lies in describing the response of a detector to a moving plasma when we have some theoretical ground for saying what the distribution function $\tilde{f}$ should look like in the plasma frame (e.g., $\tilde{f}$ might be approximately

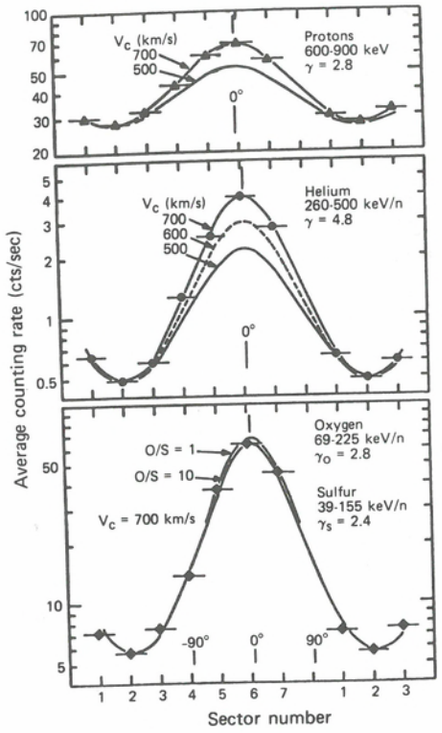

Fig. 4.10. Detailed fit of sectored data using Equation (4.5) of the text. The data represent a 73-min. average for a quiet time on the Voyager 2 inbound trajectory. The top two panels represent fits to proton and helium data. The bottom panel represents a fit using a $Z \geq 6$ channel assuming a mixture of oxygen and sulfur (O/S = 1, 10) and a convection speed of 700 km/s [Carbary et al., 1981].

Maxwellian owing to thermalizing wave/particle interactions). However, we shall see later that (4.4) can also be used without any foreknowledge of $\tilde{f}$.

The most direct application of (4.4) can be made in the energy range where the LECP instrument can identify individual ion species and measure their spectra. This is accomplished using the pulse height analysis data from the LEPT for energies $\gtrsim 0.5$ MeV/nucleon. If we assume that $\tilde{j}^a \simeq j_0^a (E_a/\tilde{E})^{\gamma_a}$, that is, an isotropic power-law differential spectrum in the vicinity of the ion total energy E_a, then (4.4) becomes [Ipavich, 1974],

$$j^a(E,\phi) = \tilde{j}_o^a \, (E_a/E)^{(\gamma_a+1)} \left(1 - 2 \, \frac{V}{v} \sin\theta \cos\phi + \frac{V^2}{v^2} \right)^{-(\gamma_a+1)} \tag{4.5}$$

where ϕ measured from the projection ($V \sin\theta$) of the convection velocity onto the scan plane of the instrument. The flux anisotropy produced by convection can be represented more simply when the convection velocity (V) is significantly less than the particle velocity. Then (4.5) can be written in the normalized form

$$\ln \frac{j^a(E,\phi)}{j^a(E,\pi/2)} \simeq 2(\gamma_a + 1) \, \frac{V}{v} \sin\theta \cos\phi + O(V^2/v^2) \tag{4.6}$$

For the outer parts of the Jovian magnetosphere where the LECP scan plane is roughly perpendicular to the local magnetic field (so $\sin\theta \simeq 1$), one can therefore make several independent estimates of the convection velocity directly from the anisotropy

amplitudes of several separate ion species and the dependence of the amplitude on velocity (energy) for each species. Figure 4.10 shows the angular distribution for protons (0.6–0.9 MeV), helium nuclei (1.0–2.0 MeV) and $Z \geq 6$ ions (1.1–3.6 MeV) during a 73-min. interval when the intensity remained relatively constant at 58 R_J on the inbound leg of the Voyager 2 trajectory [Carbary et al., 1981]. Sectors 6, 2, and 4 pointed the sensors into, away from, and perpendicular to the corotation direction, respectively. The differential energy spectra measured during this time are well represented by $j = KE^{-\gamma}$. In sector 4, approximately perpendicular to the corotation direction, $\gamma_p = 2.8$ and $\gamma_{He} = 4.8$ in the indicated energy intervals [Krimigis et al., 1981].

The expected directional dependence of the fluxes for each ion species can be computed from (4.5) using the observed power-law spectra, assuming negligible anisotropy in the plasma rest frame. The smooth curves in Figure 4.10 represent the fluxes computed from (4.5) for various values of $V \sin\theta$. An excellent fit for all sectors is obtained when $V \sin\theta = 700$ km/s for both protons and helium. The corotation velocity of $V_c = \Omega R$ is 730 km/s at 58 R_J. The remarkable agreement between the measured and computed fluxes in each of the seven sectors for particles having different velocities and spectral exponents provides strong evidence that the plasma indeed corotates rigidly at this distance from the planet. The bottom panel shows the results of a similar analysis where γ was independently determined from anisotropies of $Z \geq 6$ ions from a rate channel for which $V_c = 700$ km/s was assumed. Again, an excellent fit to the data was obtained.

Before proceeding, let us consider the assumption underlying (4.5) that $\tilde{j}^a$ was isotropic in the convected frame. It has been pointed out that spatial gradients in the distribution function and flows parallel to the local magnetic field may make significant contributions to the anisotropies measured in the Jovian magnetosphere [e.g., Northrop, Birmingham, and Schardt, 1979; Thomsen et al., 1980; Birmingham and Northrop, 1979]. For the particular example just given, Carbary et al. [1981] determined that spatial gradients were relatively small, and that the flows were essentially convective. However, the resolution of the question of gradient anisotropies is particularly important at lower energies where LEMPA provides less exact information on ion composition than does the LEPT at higher energies.

If the particle flux is not too anisotropic in some frame of reference, the first-order anisotropy produced by a spatial gradient in flux intensity is given by the well-known expression

$$\mathbf{A}_{\text{grad}} = \rho \, \hat{\mathbf{B}} \times \nabla \ln j \tag{4.7}$$

where ρ is the particle's local gyroradius (pc/qB) and j is the flux averaged over all directions. This expression may be generalized to strong anisotropies without losing its essential character as long as the anisotropies remain unidirectional [Roelof, 1975]. The essential point to remember from (4.7) is that gradient anisotropies are large only when the spatial scale of the flux perpendicular to the magnetic field gets as small as a cyclotron radius.

For comparison, the anisotropy (in the spacecraft frame) due to convection alone can be written down directly from (4.6)

$$\mathbf{A}_{\text{conv}} = \frac{2}{v} (\gamma + 1) \, \mathbf{V} + O(V^2/v^2) \tag{4.8}$$

The coefficient of $\mathbf{V}/v$ in (4.8) may be recognized as three times the "Compton-Getting Factor," well-known to cosmic-ray physicists, and A_{conv} is referred to as the "Compton-Getting Anisotropy" [see Gleeson and Axford, 1968].

It has been suggested to us that gradient anisotropies could mimic corotation anisotropies near the "neutral sheet" of Jupiter's magnetodisc. The reason given was that the cyclotron radius of partially ionized ions can become large ($>1\ R_J$) because the residual north–south field is small ($\lesssim 1\ nT$), so that a positive radial flux gradient on the scale of several R_J could produce an azimuthal anisotropy in the corotation direction. However, the data from the LECP does not support this conjecture. Carbary, Krimigis, and Roelof [1982] show that the form of the energy spectrum does not vary strongly with radius, so the $\nabla \ln j$ term in (4.7) is approximately energy independent. Consequently, A_{grad} should increase with velocity, but the measured anisotropies show no significant change between 0.1 and 1.0 MeV, a factor of 3 change in velocity. The lack of energy dependence in this energy range is more consistent with that predicted by (4.8) because the observed spectra steepen noticeably between 0.1 and 1.0 MeV, tending to keep the fraction $(\gamma + 1)/v \simeq$ constant. Moreover, as we shall see in the next section, we find anisotropies whose amplitudes and directions both are consistent with convection throughout the magnetodisc, including the immediate vicinity of the neutral sheet. We have not yet seen any evidence in the data in support of gradient anisotropies dominating convective anisotropies.

Because we have been discussing convective anisotropies for both power-law and thermal spectra, it is worthwhile comparing their energy and species dependence. For a thermal spectrum, Roelof et al. [1976] showed that convected thermal distributions have the same general dependence as given by (4.6) if γ, the local power-law exponent, is calculated from the definition $\gamma = -(\partial \ln \tilde{j}/\partial \ln \tilde{E})$ using the thermal flux $\tilde{j} = \tilde{p}^2 (2\pi mkT)^{-3/2} \exp(-\tilde{E}/kT)$

$$\ln \frac{j(E,\phi)}{j(E,\pi/2)} \simeq \frac{mvV}{kT} \sin\theta \cos\phi + O(V^2/v^2) \tag{4.9}$$

Thus both power-law and thermal convected fluxes have anisotropies obeying an approximate log-cosine law when $V << v$:

$$\ln \frac{j(E,\phi)}{j(E,\pi/2)} \simeq \alpha \cos\phi + O(V^2/v^2) \tag{4.10}$$

where $\alpha = mvV \sin\theta/kT$ for a thermal spectrum, and $\alpha = 2(\gamma + 1)(V/v) \sin\theta$ for a local power-law spectrum.

Note that the anisotropy amplitude α varies inversely with velocity for a power law, but directly with momentum for a thermal spectrum. But if we now fix the particle's total energy for ion species with different atomic mass numbers A, then $v \propto A^{-1/2}$ and $mv \propto A^{1/2}$, so we have (rather remarkably) $\alpha \propto A^{1/2}$ for either a thermal or a power-law spectrum (assuming that either T or γ is the same for all species). An immediate consequence of either (4.6) or (4.10) is that if a heavy ion species has an integral flux in the convective frame comparable to that of the protons, the forward fluxes ($\phi = 0$) in the spacecraft frame will be dominated by the heavy ions. For example, consider 20 keV ions of atomic mass number A: $\alpha \simeq A^{1/2}\gamma\ (V/1000\ \text{km s}^{-1})$ for $2 \lesssim \gamma \lesssim 4$, or for a thermal distribution, $\alpha \simeq A^{1/2}\ V/50\ kT$ (where V is in km s^{-1} and kT in keV). Then for $V = 1000$ km s^{-1}, protons would have anisotropies of $\alpha = \gamma$ or $\alpha = 20/kT$ either of which can be of order unity in the magnetodisc, while ^{16}O or ^{32}S nuclei of the same energy would have anisotropies 4 or 5.7 times stronger.

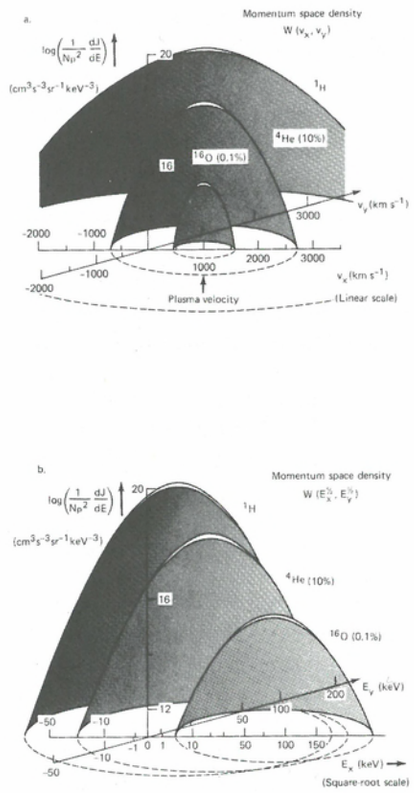

Fig. 4.11. Distribution functions and instrument response for a hot flowing plasma incident on a low energy magnetic spectrometer (LEMS), such as the ion channels of the LEMPA. Upper and middle panels show momentum-space densities of ^{1}H, ^{4}He (10%) and ^{16}O (0.1%) nuclei as a function of (*a*) particle velocity, or (*b*) total energy, for all directions relative to hot plasma flow ($kT = 5$ keV, $V = 1000$ km s^{-1}). Lower panel (*c*) shows the incident differential particle spectra for each species when the detectors look into the plasma flow; actual portions of spectra to which LEMS respond are shaded. The summed response of the LEMS is not only sensitive to hot-plasma flow, but it also displays the spectral signature (flattening) of the presence of heavy nuclei.

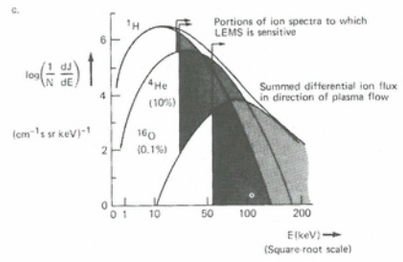

One means of visualizing the way an energetic particle detector responds to a convected hot plasma including several ion species is to represent the different components of the plasma in terms of the momentum space density $W(\mathbf{p})$, which is related directly to the plasma density $N(\text{cm}^{-3})$ and the differential unidirectional particle flux $j(E)$ through $W(\mathbf{p}) = j(E)/Np^2$. If the bulk plasma velocity is taken along the p_x direction, and if the distribution function is symmetric about this axis, we may chose p_y as the transverse momentum $p_\perp$ in an arbitrary transverse direction. Then the z axis may be used to represent the momentum space density itself $W(p_x, p_y)$, and from the momentum space density surface we can directly derive the directional dependence of the flux

incident on a detector from the intersection of the right circular cylinder $p_x^2 + p_y^2 = p^2$ with $W(p_x, p_y)$. Of course, W must be multiplied by Np^2 to obtain the true flux $j(E)$.

In Figure 4.11, we present a set of Maxwellian momentum-space densities $W(\mathbf{p})$ for the hydrogen, helium (10% abundance relative to ^{1}H) and oxygen (0.1% abundance relative to ^{1}H) components of a $kT = 5$ keV plasma moving with a bulk velocity of $\mathbf{V} = 1000$ km s^{-1}. These are shown in two novel representations in terms of energy. First, let us define as the independent variable in our first representation $(E_x/A)^{1/2} = (E_\parallel/A)^{1/2}$ and $(E_y/A)^{1/2} = (E_\perp/A)^{1/2}$, which have the same mass-independent proportionality to the velocity components $(v_x, v_y) = (v_\perp, v_\parallel)$ for all species. Because $\tilde{v} = v - \mathbf{V}$ and $\tilde{\mathbf{W}} = (2\pi mkT)^{-3/2} \exp(-m\tilde{v}^2/2kT)$, the thermal density surfaces in a log $W[(E_\parallel/A)^{1/2}, (E_\perp/A)^{1/2}]$, plot, as in Figure 4.11*a* are coaxial parabo loids of revolution centered on $(E_x/A)^{1/2} = V(m_i/2)^{1/2}$, where m_i is the average mass/nucleon, since $m\tilde{v}^2/2kT = (A/kT)[(E_x/A)^{1/2} - V(m_i/2)^{1/2}]^2 + (A/kT)(E_y/A)$. The paraboloids are broader for the lighter elements, since the e^{-1} (thermal) width is $(kT/A)^{1/2}$. Although Figure 4.11*a* portrays the more familiar aspects of a multispecies thermal distribution (characterized by a single temperature), it does not provide the insight we need into the response of instruments like the LEMPA, which measure the total energy that is deposited in the detector, not the velocity. Consequently, in Figure 4.11*b* we plot log W as a function of $E_x^{1/2} = E_\parallel^{1/2}$ and $E_y^{1/2} = E_\perp^{1/2}$. The surfaces of constant W are still paraboloids of revolution, but now they all have identical shapes because $m\tilde{v}^2/2kT = [E_x^{1/2} - V(Am_i/2)^{1/2}]^2/kT + E_y/kT$ and the thermal (e^{-1}) width is simply $(kT)^{1/2}$. However, their axes are now displaced from each other along the $E_x^{1/2}$ axis at the values $V(Am_i/2)^{1/2} \propto A^{1/2}$. It is the distribution function as shown Figure 4.11*b* that is relevant to the LEMPA response, rather than more familiar representation as in Figure 4.11*a*.

Of course, what the instrument really "sees" is the incident differential flux $j = Np^2W$, and this function is plotted for the flux (due to each of the three species) in the convection direction ($\phi = 0$) as a function of $E_x^{1/2}$ in Figure 4.11*c*. In Appendix A we describe how the actual instrument response is obtained by integrating the incident flux over the detector solid angle and energy passband efficiencies $\epsilon_k^a(E)$, and then summing over all species; see Equation (4.19) and Figure (4.31). We have given a suggestion of this all important step in Figure 4.11*c* by indicating approximately the lowest energies of the ^{1}H, ^{4}He, and ^{16}O fluxes to which the LEMPA responds (e.g., the lower extent of the ϵ_k^a for the lowest detector energy channel). Immediately one sees from the Figure 4.11*b* the very dramatic enhancement of heavy ion fluxes in the convection direction, and Figure 4.11*c* raises the possibility that ions such as ^{16}O, if their abundance approaches that of ^{1}H, could dominate the LEMPA response in the corotation direction in the Jovian outer magnetosphere. Consequently, the problems of estimating the convection velocity and deducing the composition of the hot plasma from the LEMPA channel rates are intertwined.

The exact expression for the incident integral flux due to a convected thermal distribution was calculated by Roelof et al. [1976]

$$J(E,\phi) = \pi^{-3/2} N v_0 e^{-V^2 \sin^2\phi / v_0^2} e^{y^2 - x^2} H(x,y) \tag{4.11}$$

where N is the plasma density, v is the velocity of a particle with the detector threshold energy E, v_0 is the particle velocity with energy $E_o = kT$, $x = (v - V\cos\phi)/v_0$, $y = V\cos\phi/v_0$, V is the plasma bulk velocity, and

$$2H(x,y) = x^2 + 3xy + 3y^2 + 1 + (\pi/2)^{1/2}(3y + 2y^3)\, e^{x^2}\, erfc(x) \tag{4.12}$$

Selected calculations of integral fluxes incident in the forward direction, $J(E,O)/N$, from (4.11) and (4.12) are presented in Figure 4.12 for plasma velocities above 100 km s^{-1} and temperatures from 100 to 20 keV for 20 keV protons, 15 keV electrons, 30 keV ^{4}He and 20 keV ^{12}C, ^{23}Na, and ^{56}Fe. Also included in Figure 4.12 as dashed lines are contours of the exponential anisotropy parameter $\alpha = mvV/kT$ from (4.9) which gives an approximate indication of the strong anisotropies of the fluxes. The strong dependence on temperature and bulk velocity is particularly dramatic for the heavier species.

To illustrate the sensitivity of the LEMPA detector to flowing thermal plasmas, we have plotted in Figure 4.13 the differential forward fluxes in the lowest channel of Voyager 2 versus kT for selected flow velocities of a hydrogen plasma at a density of

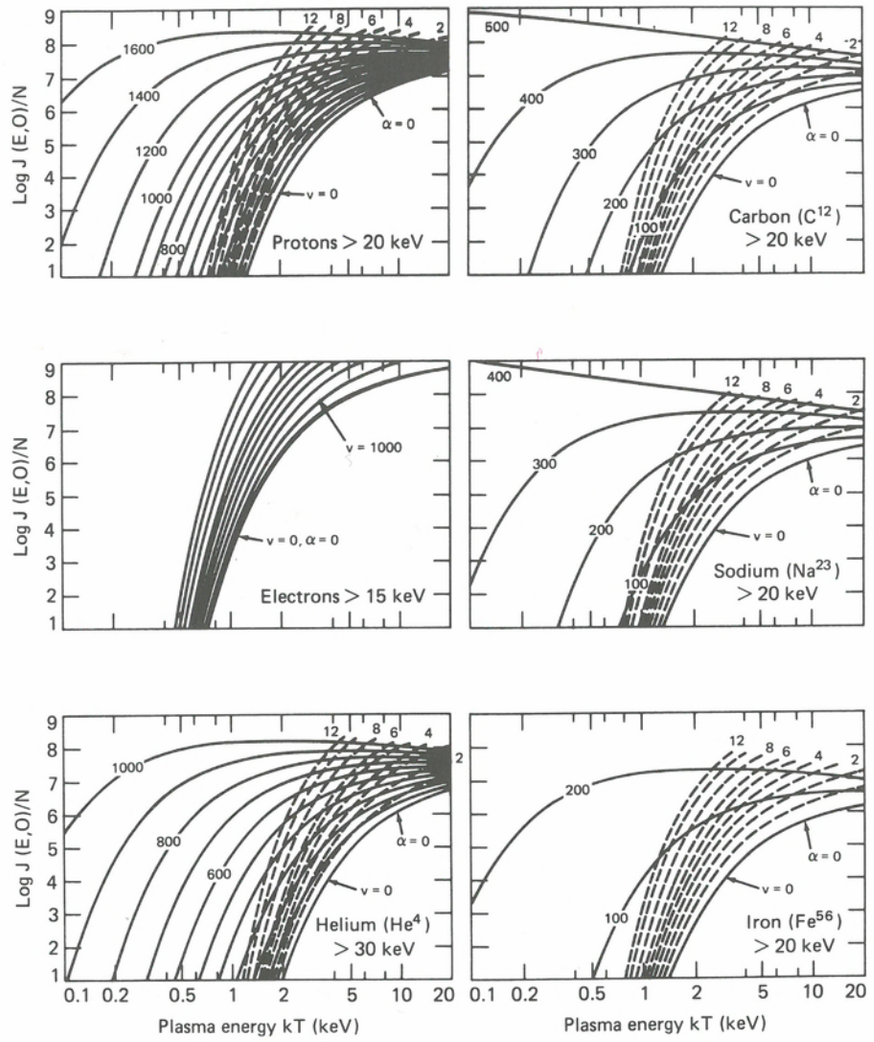

Fig. 4.12. Incident integral flux (energy > E) in the ion flow direction of thermal plasma $J(E,O)$, normalized by density of each species (N), as a function of plasma temperature (kT) for various values of plasma velocity. Dashed lines give contours of anisotropy parameter $\alpha = mvV/kT$; see Equation (4.10).

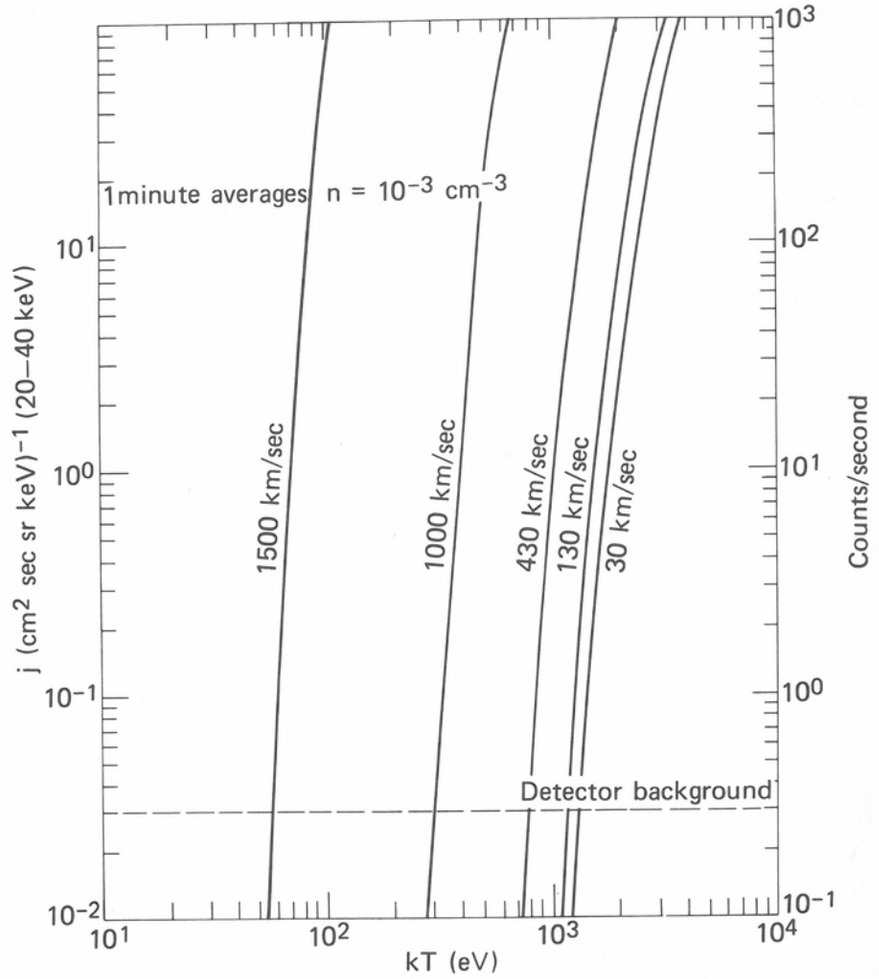

Fig. 4.13. A figure to demonstrate the ability of the LEMPA detector in responding to a very tenuous hot flowing plasma. The curves labeled by the plasma flow speed indicate the proton differential fluxes at 20–40 keV as a function of plasma temperature for a plasma with density 10^{-3} cm^{-3}. The detector background is shown to illustrate the sensitivity of the instrument. For example, for a plasma of density 10^{-3} cm^{-3} flowing at 30 km/s, the proton fluxes are above our detector background when the plasma temperature is above 1.3 keV.

10^{-3} cm^{-3}. At such low densities, most plasma instruments have difficulty in measuring plasma velocities and temperatures on relatively short timescales ($\sim$ 1 min). It is evident from the figure that LEMPA can readily measure small ($\sim$ 50–100 km s^{-1}) velocities at plasma temperatures $\gtrsim$ 1 keV, and responds to higher temperature ($\gtrsim$ 10 keV) plasma without requiring large flow velocities, even at these low densities. The presence of heavier ions enhances this sensitivity.

Krimigis et al. [1979a] made use of these dramatic ion anisotropies to identify oxygen as a major component in the Jovian magnetosphere. Shortly after the first (inbound) magnetopause crossing, the lowest energy ion channel (PL01) of LEMPA on Voyager 1 measured the angular distribution shown in the inset to Figure

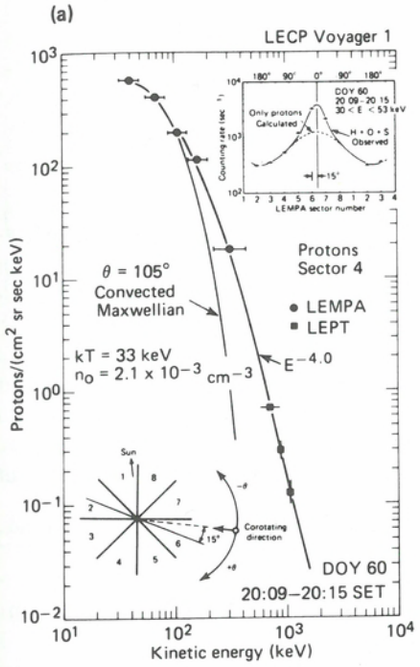

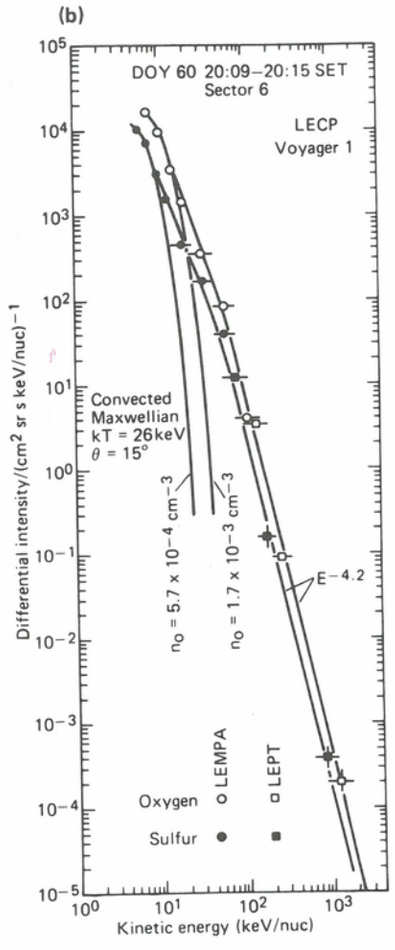

Fig. 4.14. Evidence from flux anisotropies for comparable densities of He and O: (*a*) Angular distribution in Voyager 1 LEMPA channel PL01 just inside dayside magnetopause, with LEMPA/LEPT spectrum in the sector (4) transverse to corotation fit by corotating ($V \sim 800$ km s^{-1}) thermal ($kT = 33$ keV) proton distribution with nonthermal, power-law tail ($\gamma = 4.0$); and (*b*) Spectrum from forward sector (6) with proton contribution subtracted, fit by similar distribution to (*a*), but for corotating hot O and S ions (O/S $\simeq$ 3) [from Krimigis et al., 1979a].

4.14*a*. The sector rates in the directions away from corotation (2,3,4), as well as the spectrum in the transverse direction shown in Figure 4.14*a*, can be fit by a corotating ($V \sim 800$ km s^{-1}) thermal ($kT = 33$ keV) proton distribution that makes a transition to a nonthermal power-law tail ($\gamma = 4.0$) at an energy $E \simeq (\gamma + 1)\,kT$; we discuss this "gamma-thermal" distribution in detail in Appendix B. It is clear from the inset to the figure, however, that the low-energy sectors in the direction of corotation (5,6,7) must be responding to heavier ions, in addition to the protons (dashed lines). Subtracting this proton contribution from the rates in the forward sector (4.6), and assuming the "excess" ions are oxygen and sulfur with O/S $\sim$ 3, as measured at $\gtrsim$ 200 keV/nucleon by the LEPT, a satisfactory fit is obtained in Figure 4.14*b* for essentially the same distribution parameters used to fit the protons in Figure 4.14*a*. Therefore Krimigis et al.

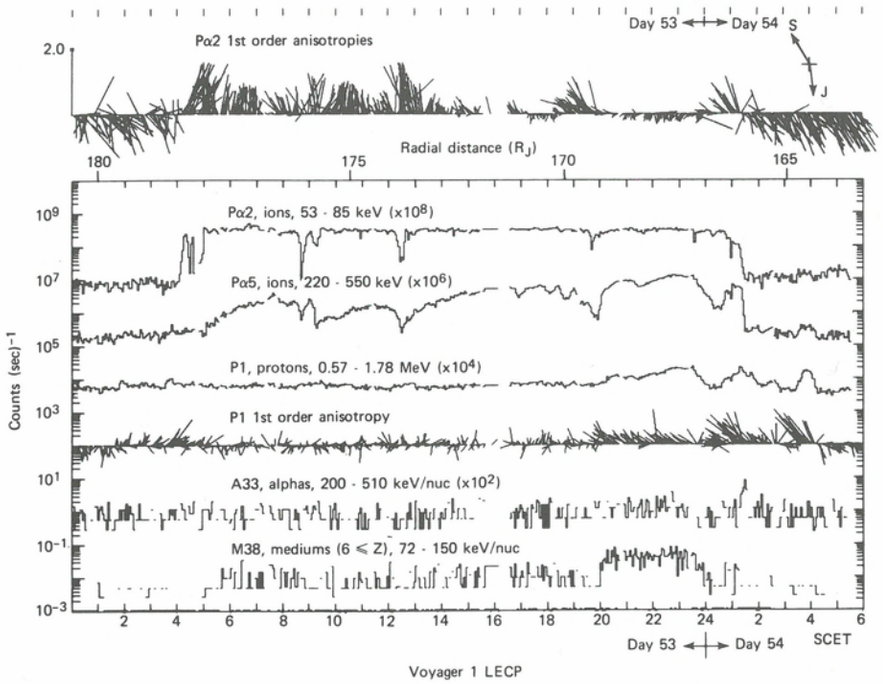

Fig. 4.15. Long-lived Jovian particle event observed on day 53 by Voyager 1 inbound. The count rate data are averaged over one scan, 192 seconds. The flat top PL02 profile is typical for long-lived events, as is the gradual rise in the PL05 count rate. A clear increase in the P1 count rate occurred after the main event on day 54 [Zwickl et al., 1981]. The anisotropy direction is noted at upper right, with arrows pointing towards the Sun (S) and Jupiter (J).

[1979a] were able to conclude that the concentrations of H and O were comparable in this region of the magnetosphere.

This then completes our presentation of techniques for deducing convection velocities and composition of flowing multicomponent plasmas. In Section 4.4, we estimate hot plasma pressures and number density. The theoretical basis of these estimates can be found in Appendix C.

4.4. Presentation of results

Upstream regions

As noted in connection with Figure 4.3, the first inbound observation of a "Jovian Ion Event" occurred at $\sim 600\ R_J$ on Voyager 1 and $\sim 860\ R_J$ on Voyager 2, although outbound observations by Voyager 1 show small ion events to beyond $1200 R_J$. Although not shown here, the maximum flux level of the short-lived events falls off slowly with increasing radial distance as does their frequency [Zwickl et al., 1981].

Figure 4.15 presents the details of one long-lived event observed by Voyager 1 on day 53, 1979 at a distance of $\sim 175\ R_J$ upstream from Jupiter [Zwickl et al., 1981]. The flux profile of the lowest energy ions in $P\alpha 2$ has a rapid onset followed by a nearly constant flux level for ~ 21 hr, then displays an equally rapid decay. Several of the short-lived decreases observed in the flux of the $P\alpha 2$ time profile occurred during the passage

of what appear to be tangential discontinuities (TD's) in the interplanetary magnetic field, which was nearly radial throughout this event (N. F. Ness, private communication, 1981). Note that these decreases tend to occur at 5-hr intervals, suggesting Jovian magnetosphere control throughout the event. The connection, if any, between the TD's and the suggested periodicity is not understood. The ion anisotropy at 53 keV changes abruptly at event onset from a solar convective direction to a direction consistent with flow outward away from Jupiter as shown in the vector plot on top of the figure. The anisotropy magnitude is initially very large but decays with time. In this event, the flow direction of 53 keV ions actually reverses to an inward flow later in the event. The higher energy ions have a much slower onset whereas the more energetic protons in channel P1 do not increase until 2000 hr on day 53, that is, toward the end of the event. Note that the spectrum becomes harder at this time, and actually exhibits a peak at about 500 keV early on day 54 [Zwickl et al., 1981].

There are other aspects of this event, however, that are worth noting. First, the alpha particle intensity shown in channel A33 remains essentially at preevent background throughout this entire period while the $Z \geq 6$ ion population (channel M38) shows an increase at the beginning of the event and again at about 2000 UT, suggesting that the lower energy ions in $P\alpha 2$ and $P\alpha 5$ are primarily $Z \geq 6$. As noted in Figure 4.3, pulse-height analysis spectra at ~ 0.5 MeV/nucleon during the later part of this event show the higher energy ions to consist primarily of oxygen and sulfur. Because this composition is known to be characteristic of ions within the Jovian magnetosphere, we are led to suggest that upstream events are probably due to ions escaping directly from the magnetosphere. In view of the complexity of the structure, however, and the strange intensity-time profile, which are not unlike those observed upstream from Earth [Sarris et al., 1978; Scholer et al., 1980], there could well be additional mechanisms at work.

Outer magnetosphere

Magnetosheath-magnetopause. Scan-averaged (192 s) ion and electron count rates and first-order particle anisotropies are shown in Figure 4.16 for the interval around the first magnetopause crossing by Voyager 1 [Krimigis et al., 1979a]. The ion rates are enhanced immediately behind the bow shock and the anisotropy vectors initially point in the direction of the deflected solar wind. The ion count rate in the magnetosheath is at a level that is essentially identical to that observed during the long-lived upstream ion event on days 53 and 54. As the spacecraft approached the magnetopause, we note that the anisotropy becomes more radial in nature, that is, ions flow away from Jupiter. Upon crossing the magnetopause, the flows changed from the radial to the corotational direction. Details of the particle count rate in each sector at selected time intervals during the magnetopause crossing are shown as insets to Figure 4.16. Prior to magnetopause crossing, the flow was directed away from Jupiter; during the crossing, the flow began to change to a corotational direction; after the crossing, the flow was strongly corotational. This convective flow in the corotational direction is characteristic of most plasma flow in the Jovian magnetosphere both on the dayside and nightside, as previously summarized in Figure 4.7. The magnetopause crossing for the electrons is much better defined than for the ions.

Energy spectra. As explained in Section 4.3, it is possible to use the angular and spectral measurements of the LECP instrument to deduce the temperature at lower energies (i.e., $\lesssim 200$ keV) and the spectral slope at higher energies ($\gtrsim 200$ keV) throughout the magnetosphere, all in the rest frame of the plasma. Figure 4.17 pre-

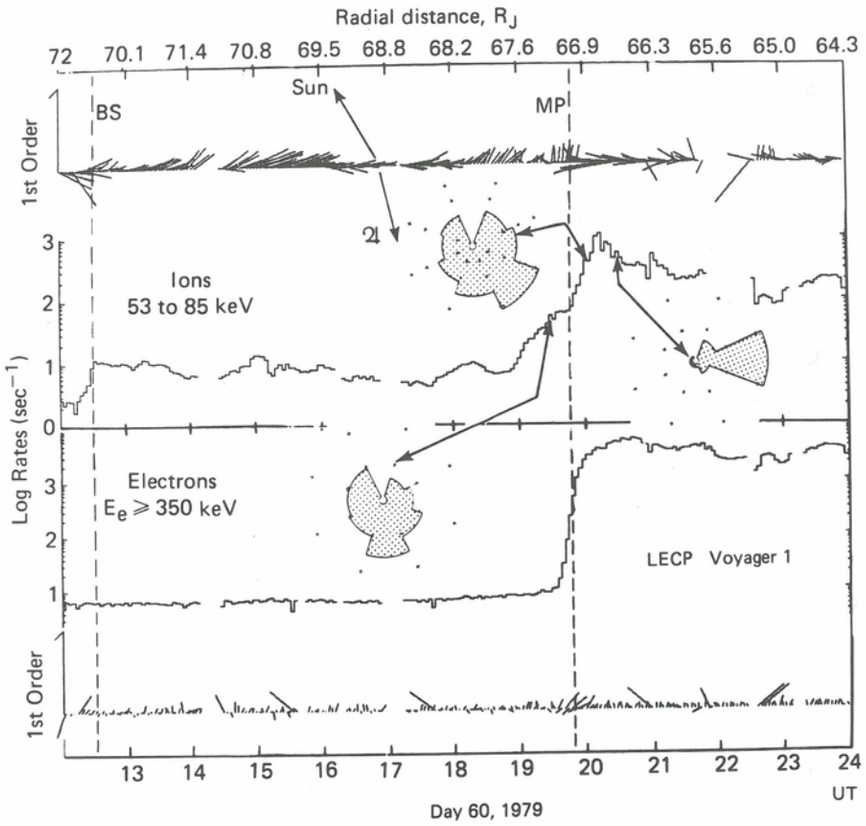

Fig. 4.16. Particle intensities and flows around the interval of the first magnetopause crossing. Pie diagrams at selected points show detector count rate as a function of view direction [Krimigis et al., 1979a]. Note that some radial outflow is observed, notably at ~2230 to 2300 UT.

sents the results of these computations for the inbound pass of Voyager 1 using 15-min. count rate averages. The top panel shows the count rate for 53–85 keV ions averaged over the detector scan and includes the nominal crossing times of the magnetic equator. The middle panel shows the spectral exponent γ; the spectra tend to be softer (larger γ) at magnetic equatorial crossings, especially in the outer magnetosphere, with systematic spectrum variations well over 1 unit of γ. The amplitude of the fluctuations is considerably reduced after the final magnetopause entry at the beginning of day 62.

The lower panel displays the calculated proton temperature kT; there appears to be a significant correlation between peaks in the temperature profiles and times of crossing of the magnetic equator. Specifically, on days 62–63 the four major peaks are ~10 hr apart and occur at the $\lambda_{III} \sim 300°$ crossings (active sector, see Chap. 10); corresponding peaks at $\lambda_{III} \sim 100°$ crossings are more difficult to discern. There are however exceptions to this general correlation, the most obvious of which is the temperature peak at 1700 UT on day 63. Undoubtedly there exist time variations that can distort the apparent association between equatorial crossings and kT, as evidenced by the Voyager 2 encounter [Krimigis et al., 1981]. In general it can be stated that the temperature increases at the equator and decreases at high latitude, and is thus anticorrelated with the spectral behavior of the power law at higher energies.

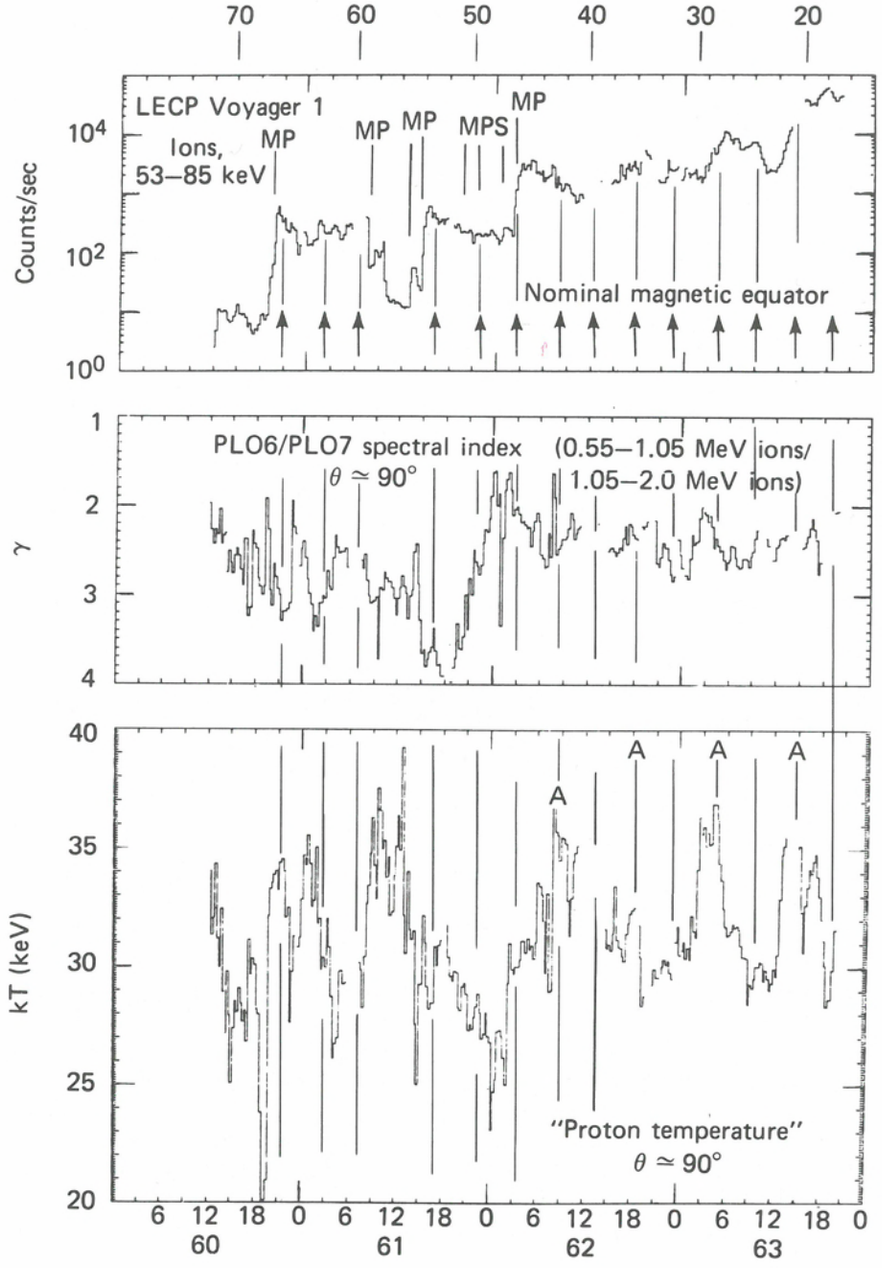

Fig. 4.17. Voyager 1 inbound spectral parameters [Krimigis et al., 1981]. The lower panel displays the calculated proton temperature derived from 15 min. averaged data from the sector perpendicular to the flow direction. The second panel shows the spectral index derived from the PL06 and PL07 channels in the same sector. The top panel shows the counting rate of the PL02 channel and includes the magnetopause (*MP*), bowshock (*S*), and nominal magnetic equator crossings (arrows). *A* indicates the active sector, $\lambda_{III} \sim 260°$ (see Chap. 10).